

## Article

# Sustainable Removal of Ammonia from the Anaerobic Digester Supernatant Line Using a Prussian Blue Analogue (PBA) Composite Adsorbent

Paz Nativ  <sup>†</sup>, Zenebu Abera Derbew <sup>†</sup>, Chen Dagan-Jaldety, Yaron Aviezer, Raz Ben-Asher and Ori Lahav <sup>\*</sup>

Faculty of Civil and Environmental Engineering, Technion, Haifa 3200003, Israel

\* Correspondence: agori@technion.ac.il

† These authors contributed equally to this work.

**Abstract:** This paper reports on the physico-chemical removal of  $\text{NH}_4^+$  from the supernatant line in municipal wastewater treatment plants (WWTPs), using zinc-hexa-cyano-ferrate (ZnHCF) beads. The work is divided into three parts: First, the characteristics of three (Zn-, Co-, Ni-) types of HCF beads were determined, with a finding that ZnHCF was the most suitable for the purpose of this work. Second, synthetic and actual supernatant wastewater was passed through a ZnHCF column for many cycles until apparent steady-state results were attained. Due to the very high affinity of the beads toward  $\text{NH}_4^+$  and the much lower affinity toward competing cations, the same regeneration solution could be used for many cycles (20 cycles in this work) without affecting the following adsorption breakthrough curve efficiency and the operational capacity, which was >88% at the end of all adsorption steps. Finally, a cost analysis was performed, revealing that the cost of removing ~500 mg/L of ammonia from the supernatant line is ~\$0.02 per m<sup>3</sup> of raw wastewater flowing into the plant if the ammonia is recaptured and sold as  $\text{NH}_4\text{Cl}$ . This may be cost-effective when the WWTP receives a higher-than-planned load, and an incentive exists for alleviating the ammonia load on the oxidation reactor.

**Keywords:** ammonia; dewatering supernatant; digested sludge; Prussian Blue Analogues (PBA) composite; separation; WWTP



**Citation:** Nativ, P.; Derbew, Z.A.; Dagan-Jaldety, C.; Aviezer, Y.; Ben-Asher, R.; Lahav, O. Sustainable Removal of Ammonia from the Anaerobic Digester Supernatant Line Using a Prussian Blue Analogue (PBA) Composite Adsorbent. *ChemEngineering* **2022**, *6*, 97. <https://doi.org/10.3390/chemengineering6060097>

Academic Editor: Alírio E. Rodrigues

Received: 28 November 2022

Accepted: 13 December 2022

Published: 15 December 2022

**Publisher's Note:** MDPI stays neutral with regard to jurisdictional claims in published maps and institutional affiliations.



**Copyright:** © 2022 by the authors. Licensee MDPI, Basel, Switzerland. This article is an open access article distributed under the terms and conditions of the Creative Commons Attribution (CC BY) license (<https://creativecommons.org/licenses/by/4.0/>).

## 1. Introduction

Separation for reuse or the oxidation of Total Ammonia Nitrogen (TAN) from the supernatant flow of anaerobic digesters in municipal wastewater treatment plants (WWTPs) has been suggested by a variety of methods. Some of these methods are biological, such as oxidation by anammox bacteria [1–5], and others physico-chemical, such as struvite precipitation [6–8], advanced oxidation processes (AOPs) [9,10], and adsorption-desorption cation-exchange (CIX) sequence [11–13]. Since the TAN concentration in the supernatant stream is typically high (300–1300 mgN/L) and has no daily fluctuations, the conditions are advantageous, kinetic-wise, for ammonia removal. Treating this stream has the benefit of alleviating the ammonia load on the main WWTP oxidation reactors, which may be important when the main oxidation reactor is highly loaded, or when rising sludge episodes are encountered [14] due to an excessively long sludge age [15,16].

Ion exchange may be an advantageous process for the removal of  $\text{NH}_4^+$  from wastewater (WW) because of the high affinity of certain resins/zeolites toward  $\text{NH}_4^+$ , the short retention time (typically a few minutes) that is required, its simple operation, and the high removal efficiency that can be attained at a wide range of temperatures and concentrations. However, to be economically feasible, the regeneration solution should undergo  $\text{NH}_4^+$  removal so it can be reused for many cycles, (ideally) replenishing only the  $\text{Na}^+$  mass that is lost for  $\text{NH}_4^+$  during the adsorption step [13]. The removal of  $\text{NH}_4^+$  from high-concentration CIX regeneration solutions has been addressed in several works by

using physico-chemical approaches such as stripping [17], O<sub>3</sub> oxidation [18], and indirect electrochemical oxidation [13,19,20]. A comparison between the main techniques used to date for removing ammonia from the dewatering supernatant stream is presented in Table 1.

**Table 1.** Comparison of varied methods for ammonia removal and reuse from WWTP dewatering supernatant (three ✓ = high).

Method	Technological	Feasibility Cost	Reliability	Readiness Level	Source
Anammox	✓✓✓	✓	✓✓	✓✓✓	[2,3]
CIX-Zeolite	✓✓	✓✓✓	✓✓✓	✓✓	[12,13,21,22]
CIX-CuHCF	✓✓	✓✓✓	✓✓✓	✓✓	[11]
Struvite precipitation	✓✓✓	✓✓	✓✓✓	✓✓✓	[7,8,23]
Current method	✓✓✓	✓✓✓	✓✓✓	✓✓✓	This paper

The immediate drawback of conventional ion exchange operations is that often the affinity of commercial cation exchange resins toward both Ca<sup>2+</sup>/Mg<sup>2+</sup> and K<sup>+</sup> is higher than the affinity toward NH<sub>4</sub><sup>+</sup> [24–26]. This may result in the low operational capacity of the breakthrough curves and, as a result, in frequent need to replace the regeneration solution due to the accumulation of the counter cations within it, which would result in a deterioration in the CIX capacity over time [13]. Therefore, an ion-exchange resin with a very high affinity towards ammonium is desirable due to the greatly extended duration in which the regeneration solution could be used. In the context of wastewater treatment, this is the only way to render the CIX operation cost-effective, because otherwise, the cost of replacing the regeneration solution chemical becomes prohibitive.

Possible candidates for a high-affinity NH<sub>4</sub><sup>+</sup> adsorbing material are members of the transition metal hexacyanoferrate (Me-HCF) crystal group, sometimes termed Prussian Blue analogs (PBA). Me-HCFs are coordination polymers composed of transition metal ions with coordinated CN bridges. Me-HCFs are currently used in a variety of applications, e.g., as the active material in Na<sup>+</sup>-ion batteries [27,28] and as ion-exchange material for selective adsorption of Cs<sup>+</sup> [29], Rb<sup>+</sup> [30], and NH<sub>4</sub><sup>+</sup> [11,31]. For ion exchange applications, a major advantage of Me-HCFs is their extremely high selectivity towards specific monovalent cations (the general affinity sequence is Cs<sup>+</sup> > Rb<sup>+</sup> > NH<sub>4</sub><sup>+</sup> > K<sup>+</sup> >> Na<sup>+</sup> > Li<sup>+</sup> [32]), which allows them to adsorb NH<sub>4</sub><sup>+</sup> even in the presence of a very high ionic background (for example under a high Ca<sup>2+</sup>, Na<sup>+</sup>, and K<sup>+</sup> background [33]).

The current work focused on the separation of NH<sub>4</sub><sup>+</sup> ions from the supernatant line of a WWTP using a composite Me-HCF-packed bed column. The purpose was to validate the hypothesis that the regeneration solution can be used for many cycles without the need for replacement, and with no deterioration in the ammonia adsorption capacity and kinetics. After separating the NH<sub>4</sub><sup>+</sup>, the ammonia can be either volatilized (at high pH) and reused or oxidized to benign N<sub>2(g)</sub> using the indirect ammonia electro-oxidation process, which is an efficient method in the presence of a high Cl<sup>-</sup> concentration. Both methods for TAN removal were tested in this work, with the stripping method being simulated, while the electrochemical oxidation was performed empirically in the lab to remove the ammonia from the regeneration solution and allow its continuous reuse.

Figure 1 shows the sequence of treatment that is applied in conventional WWTPs [34] while delineating the proposed process location in the overall process scheme.

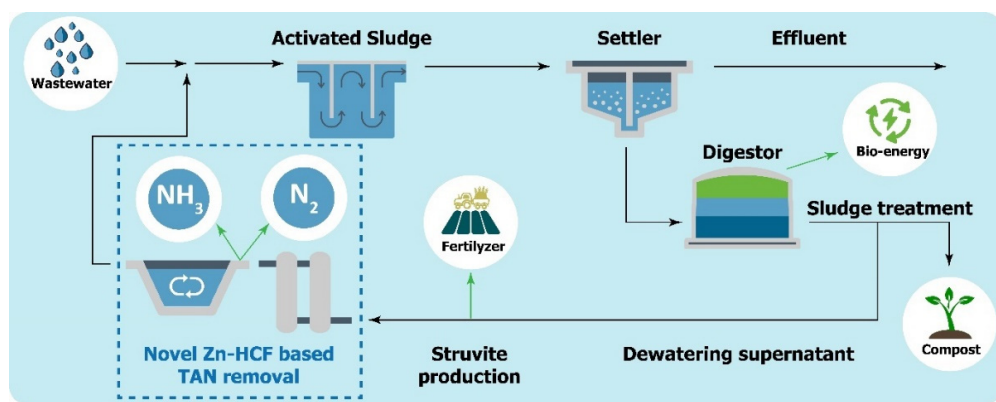


**Figure 1.** Scheme of the wastewater treatment process, showing the proposed process placement, with struvite production on the supernatant stream [35].

## 2. Materials and Methods

The work was divided into two parts: (1) characterization of the self-synthesized adsorbing materials and selection of the right candidate for the purpose of the work; and (2) finding the working conditions that would lead to stable long-term operation at the lowest possible cost.

### 2.1. Part 1: Characterization of the Adsorbing Material

#### 2.1.1. Preparation of the Me-HCFs and Beads

The Metal-HCF crystals were prepared following the procedure described in [36]. Aqueous 0.5 M solutions of Cobalt/Nickel/Zinc chloride and potassium hexacyanoferrate ( $K_4[Fe(CN)_6] \cdot 3H_2O$ ) were mixed at a 3:2 ratio. The slurry was then centrifuged, washed with deionized water (DIW), and dried, followed by grinding and sieving (Mesh #35). The resulting powders are denoted Co/Ni/Zn-HCF in the following text.

The composite beads were prepared by the method described in [33]. Polyethersulfone (PES) (BASF Ultrason E grade 6020P) flakes were dissolved in N-Methyl-2-pyrrolidone (NMP) and the Me-HCF powder (weight ratio of 1:4 of polymer to Me-HCF powder) was mixed into the dissolved polymer until homogeneous. The production of the composite bead was done using the phase inversion technique, by applying controlled precipitation of the PES mixture in a room-temperature aqueous bath.

#### 2.1.2. Isotherms

The adsorption isotherms were determined using three replicates of 125 mg Me-HCF in the form of composite beads (20% PES (*w/w*)) that were placed for 48 h in 50 mL solution at a range of initial  $[NH_4^+]$  concentrations at 25 °C in deionized water (DIW) and seawater (SW) background. The adsorption capacity ( $q$ , mgN/g Me-HCF) was then calculated using Equation (1):

$$q = (C_0 - C_i) \cdot \frac{V}{m} \quad (1)$$

where  $C$  is the initial and time-dependent (0 and  $i$  notations, respectively)  $NH_4^+$  concentration (mgN/L);  $V$  is the solution volume (L); and  $m$  is the mass of Me-HCF (g).

#### 2.1.3. Isotherm Adsorption Models

The Langmuir sorption model (Equation (A1)) fitted the isotherm experimental data well [37,38]. The  $R^2$  parameter was used to compare the model with the measured results, with a target value approaching unity.

#### 2.1.4. Morphology and Surface Area Characterization of the Me-HCF Powder and Beads

The surfaces of the ZnHCF powder and PES-ZnHCF beads were examined using high-resolution scanning electron microscopy (SEM, Ultra-Plus FEG-SEM, Zeiss, Oberkochen,

Germany). The surface area was evaluated via the Brunauer–Emmett–Teller model (BET), applied to an N<sub>2</sub> adsorption–desorption isotherm at 77 K (Quantachrome Autosorb LX4 surface area analyzer, Boynton Beach, FL, USA). Degassing of the samples at 80 °C for 12 h preceded the adsorption isotherm measurement.

#### 2.1.5. Ion Exchange Capacity and Cation Affinity Sequence

Using a batch-based adsorption technique with Cs<sup>+</sup> pre-attached onto the ZnHCF powder, the total ion exchange capacity was determined to be 2.4 meq/g (results not presented). This measured capacity of the Zn-cyanoferrate is consistent with similar values in the literature [32,39].

A sample of 0.1 g of ZnHCF powder loaded with Na<sup>+</sup> ions was used to determine the separation factor ( $\alpha$ ) in a binary component system. The background solution was simulated WWTP supernatant (1 g/L NaCl) with 5 mM of either NH<sub>4</sub><sup>+</sup> or K<sup>+</sup>. The solution was set at a constant temperature of 25 °C and stirred for three days. The separation factor was calculated using Equation (2):

$$\alpha_{Na^+}^{X^+} = \frac{(X^+)_{eq} \cdot (Na^+)_{ads}}{(Na^+)_{eq} \cdot (X^+)_{ads}} \quad (2)$$

where  $\alpha_{Na^+}^{X^+}$  is the separation factor between Na<sup>+</sup> and NH<sub>4</sub><sup>+</sup> or K<sup>+</sup> represented by X<sup>+</sup>; ( )<sub>eq</sub> is the equilibrium concentration in the bulk solution; and ( )<sub>ads</sub> is the adsorbed concentration, calculated using the total ion exchange capacity.

#### 2.1.6. Simulation of a ZnHCF-Composite Bead Packed Column

To predetermine the theoretical working conditions for the ZnHCF-composite bead column, a simulation was performed using the PHREEQC software [40] (using the transport model, Phreeqc.dat database) with the results of the separation factors and capacity of the ZnHCF adsorbent obtained by the data of the current study. The NH<sub>4</sub><sup>+</sup> adsorption and regeneration processes were simulated using the initial concentrations of the Synthetic WW1 (Table 2) with varying NaCl concentrations (0.5, 1, 1.5, 2.5, 3, 4, 5, and 6 M) in the regeneration process.

**Table 2.** Relevant concentrations of cations in the solution used in the 2nd part of the work.

Cation	Synthetic WW 1 mg/L	Synthetic WW 2 mg/L	1st Batch RWW mg/L	2nd Batch RWW mg/L
Na <sup>+</sup>	1000	185	230	245
K <sup>+</sup>	0	184	157	138
NH <sub>4</sub> <sup>+</sup>	600	600	542	566
Ca <sup>2+</sup>	0	11	30	57
Mg <sup>2+</sup>	0	35	41	29

#### 2.2. Part 2: Selection of the CIX Working Conditions

##### 2.2.1. Wastewater Solution

The supernatant of the dewatering step of the anaerobic digester sludge was obtained from the line flowing back to the oxidation reactor following the sludge dewatering step (centrifuge) in the Haifa (Israel) WWTP. The wastewater was then filtered using a gravitational sand filter (D = 1 mm) and maintained at 4 °C until use. The composition is given in Table 2.

##### 2.2.2. Column Experiments

A column packed with ZnHCF composite beads (Bed volume (BV) = 442 mL, 195 g of ZnHCF powder in the form of composite beads, I.D = 3.2 cm, H = 55 cm) was used for all the following experiments. No beads were replaced or added after the initial pack. Between the adsorption and regeneration steps, the column was rinsed with five liters of DIW.

The full experimental scheme process is described in Figure 2.

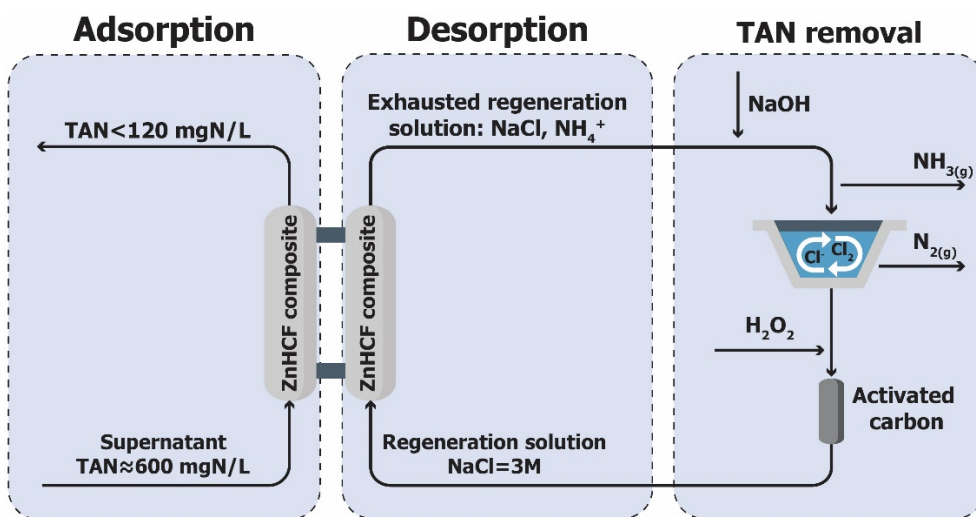


**Figure 2.** The process scheme, showing the three main steps: (1) adsorption of TAN from the supernatant water to reach an accumulated TAN concentration of ~120 mgN/L; (2) desorption of the ammonium into a regeneration solution to prepare the resin for reuse; and (3) stripping and/or electrochemical indirect oxidation of the desorbed ammonium ions into ammonia gas or benign nitrogen gas (N<sub>2</sub>), respectively, to treat the exhausted regeneration solution and prepare it for the next regeneration cycle.

#### 2.2.3. Determination of the Required Hydraulic Retention Time

Breakthrough curves were performed using a synthetic wastewater (WW1, Table 2) solution ([NH<sub>4</sub><sup>+</sup>] = 600 mgN/L, [NaCl] = 1 g/L), at varying flow rates of 0.5, 1, 2, 4, and 8 BV/h. The regeneration of the column was performed using a 6 M NaCl solution, at the same retention time used in the adsorption step. The initial results from the experiment performed with a retention time of 0.5 BV/h while setting a threshold of 120 mgN/L accumulated concentration, were used to set a 22 BV adsorption step length (see Figure A1) and a 7 BV regeneration step (the preliminary results are not shown).

#### 2.2.4. Reusing the Regeneration Solution—Full Adsorption/Regeneration Cycles

Ten full cycles were performed using a synthetic WW2 (Table 2), according to the process scheme depicted in Figure 2. From the previous step, a 3 BV/h flow rate was set, with 22 BV per adsorption cycle. For the regeneration, a 3 M NaCl solution was used in these experiments, with a 24 BV regeneration cycle. The Regeneration Efficiency (R.E) was calculated according to Equation (3):

$$R.E = \frac{V_{reg} \cdot C_{reg_f}}{V_{ads} (C_{feed} - C_{ads_f})} \quad (3)$$

where  $V_{ads}$  and  $V_{reg}$  are the volumes of the adsorption and regeneration solutions,  $C_{feed}$  is the adsorption feed TAN concentration, and  $C_{reg_f}$  and  $C_{ads_f}$ , are the final TAN concentration of the adsorption and regeneration solutions, respectively. Following that, an additional ten cycles were conducted using two batches of real WW (see Table 2 for composition). The TAN concentration in the real WW was adjusted to ~600 mgN/L by the addition of NH<sub>4</sub>Cl.

#### 2.2.5. Analyses

TAN was determined using the salicylate method [41]. Cations (and S and P) were determined using a PlasmaQuant PQ 9000 Elite, High-Resolution Array ICP-OES (Analytik Jena AG, Jena, Germany). Free chlorine was measured via a kit (HACH—method 8021).

All chemicals used were of analytical grade. DIW with conductivity < 0.9  $\mu\text{S}/\text{cm}$  was used.

### 3. Results and Discussion

#### 3.1. Part 1: Characterization of the Adsorbing Material

##### 3.1.1. Adsorption Isotherms

The purpose of the first part was to find a suitable (technically and cost-wise) metal-HCF adsorbent material that would serve to significantly reduce the TAN concentration in the effluent of the sludge dewatering step following anaerobic digestion in WWTPs.

Initially, three types of PBAs were tested: Zn, Ni, and CoHCF. Isotherms for the three adsorbents with DIW and SW as background were performed and the data points were used to model the adsorption, using the Langmuir isotherm (see Figure 3). SW was used as an example of a natural water source with a high concentration of competing cations ( $\text{Na}^+$  and  $\text{K}^+$ ). The results showed that the total capacity of Co, Ni, and ZnHCF in DIW and SW was 59.9, 27.7, and 28.5, and 60.6, 30.8, and 26.5 (mgN/gMeHCF), respectively. Looking at derived Langmuir equilibrium constant values ( $K_L$ , Table 3), a clear difference is apparent between the DIW and SW results (almost an order of magnitude) for the Co- and ZnHCF adsorbents, while a similar value was obtained for the NiHCF. The results indicate that the NiHCF adsorbent has an extremely high affinity towards ammonium ions vs. sodium ions (selectivity coefficient). Overall, the results suggest that: (1) Cobalt has the highest capacity of the tested MeHCFs, regardless of the sodium background; (2) The presence of competing ions strongly affects the operational capacity of the Zinc- and Cobalt-HCF; (3) Nickel shows little to no interference with competing ions—suggesting too-high an affinity toward ammonium over sodium, which indicates that an extreme concentration of  $\text{Na}^+$  would be required to regenerate the beads back to the  $\text{Na}^+$ -adsorbed state, which is a disadvantage.

**Table 3.** Results of the regression calculation of the Langmuir model parameters for the isotherms data (Figure 3) for Co-, Ni-, and Zn-HCF in DIW and SW background.

Background	Metal	$q_{\text{e}}^{\text{max}}$ mgN/g	$K_L$ L/mg	$R^2$
DIW	Cobalt	59.88	0.1170	0.989
	Nickel	27.72	0.0251	0.942
	Zinc	28.52	0.3967	0.969
SW	Cobalt	60.56	0.0140	0.954
	Nickel	37.13	0.0229	0.942
	Zinc	26.47	0.0104	0.985

Combined, the results suggest that the best candidate for the purpose of the work is the ZnHCF adsorbent. NiHCF was discarded due to its overly high affinity towards ammonium, which makes the regeneration step challenging or inefficient, while CoHCF's high capacity made it a suitable candidate, but the relatively small difference between the equilibrium constant determined with DIW and SW background, as compared to ZnHCF (Table 3), and the fact that the slopes of the isotherms at the lower concentration range (Figure 3B,C) were less favorable, raised concerns associated with a problematic regeneration step.

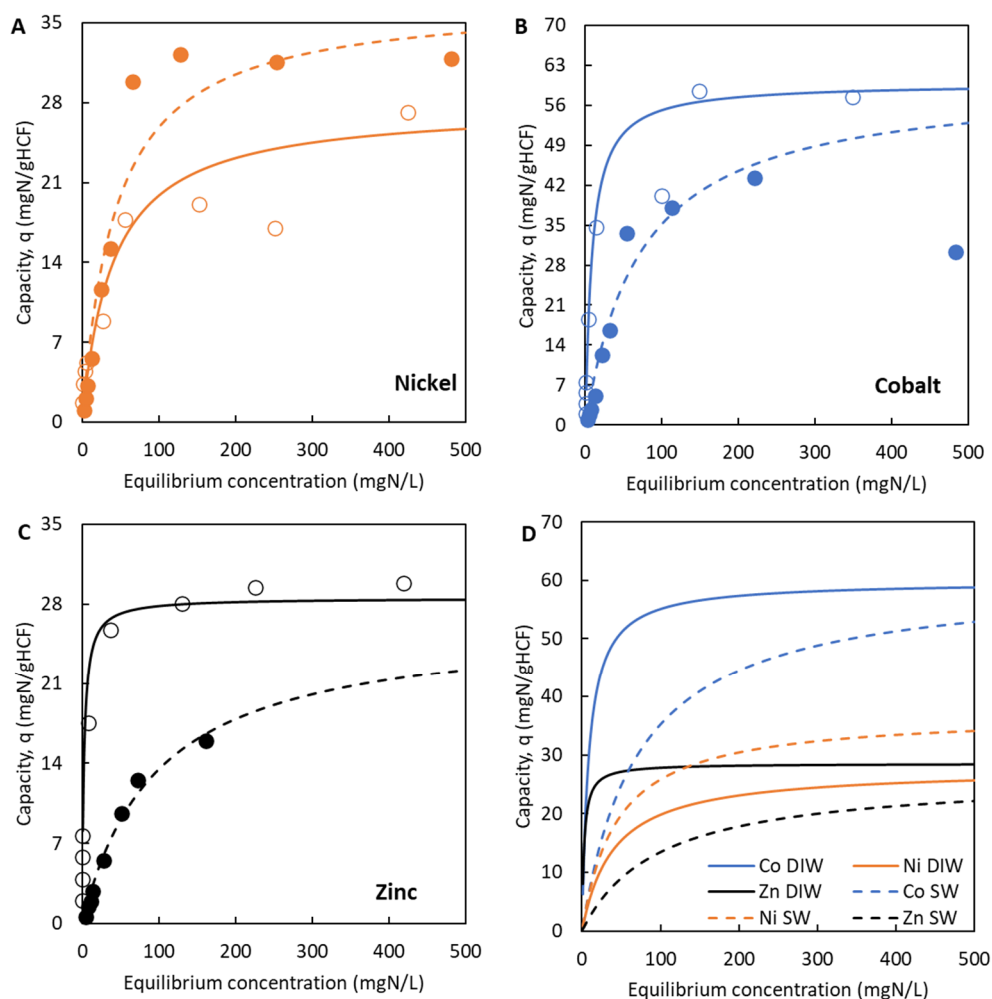


**Figure 3.** Isotherms performed on the three chosen MeHCFs. Dots indicate empirical results (empty circle—DIW, filled circle—SW); lines indicate the Langmuir model simulation (solid line—DIW, dashed line—SW). (A) NiHCF; (B) CoHCF; (C) ZnHCF; and (D) showing only the Langmuir model regression of all Me-HCFs (Dashed lines—SW, solid lines—DIW). Temperature =  $25 \pm 1^\circ\text{C}$ ,  $n = 3$ .

### 3.1.2. Characterization of the ZnHCF Beads

The selected adsorbent, ZnHCF, was analyzed to determine its compatibility with the purpose of the work, i.e., to adsorb ammonium ions from low salinity WW and its following regeneration using a recycled 3 M NaCl solution.

The typical cubic structure of the cyanoferrate was apparent in the SEM photos of both the ZnHCF powder (Figure 4A) and PES-ZnHCF beads (Figure 4B). The size and variability of the ZnHCF crystals were not affected by the presence of PES. The average bead diameter was found to be  $\sim 3$  mm, as can be seen in Figure 4C. The specific surface area was measured, using the BET method, to be  $37.0 (\pm 9)$  and  $48.5 (\pm 10)$   $\text{m}^2/\text{g}$  ZnHCF for the ZnHCF powder and PES-ZnHCF, respectively. As shown in Nativ et al. [33], the ammonium adsorption capacity does not vary in the transition from ZnHCF powder to PES-based beads (results not presented). These results are consistent with the similar surface areas of the two materials.

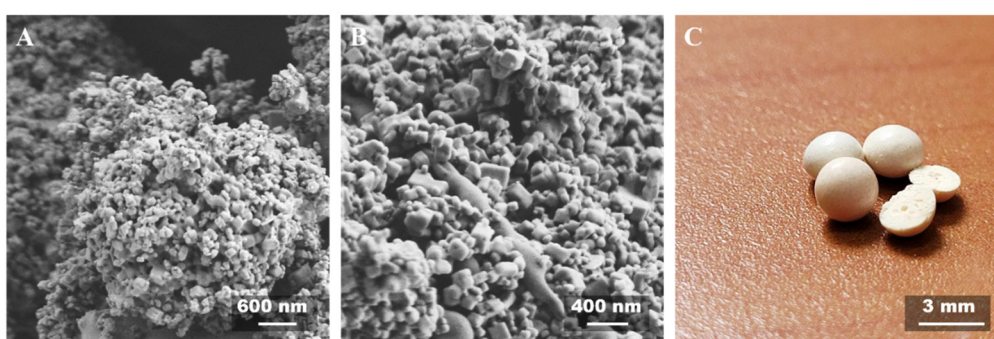


**Figure 4.** High-resolution scanning electron microscopy (HRSEM) images of ZnHCF. (A) SEM images of ZnHCF powder. (B) SEM images of PES-ZnHCF beads. (C) PES-ZnHCF beads.

The separation factor ( $\alpha$ ) values were measured with a background solution made of simulated WWTP supernatant. According to the literature, the value of  $\alpha$  is not constant but varies due to changes in the crystal structure (such as the divalent metal in the Me-HCF lattice), the pH, and temperature values, as well as the bulk solution ionic strength [31,39,42,43]. The measured separation factors (with sodium as the reference cation) determined in this study are  $\text{Na}^+:\text{K}^+:\text{NH}_4^+ \rightarrow 1:28 (\pm 4.8):101 (\pm 29)$ . The results delineate the ZnHCF's high affinity to  $\text{K}^+$  and specificity toward  $\text{NH}_4^+$ . They are also consistent with the known cyanoferrate selectivity sequence ( $\text{Cs}^+ > \text{Rb}^+ > \text{NH}_4^+ > \text{K}^+ > \text{Na}^+$  [32]) and with other separation factor values reported in the literature [31,42].

Jiang et al. and Vlasselaer et al. [31,42] both reported separation factors for Me-HCF of  $\text{Na}^+:\text{K}^+$  of 1:50 and  $\text{Na}^+:\text{NH}_4^+$  of 1:96.2 (for ZnHCF and CoHCF, respectively). These results, although measured under different working conditions and with different Me-HCFs, are similar to our findings.

The results of the PHREEQC software simulation (Figure 5A) showed that the target accumulated TAN concentration of 120 mgN/L should be attained after 26 BV, at which condition 96.7% of the adsorbing sites would be occupied by  $\text{NH}_4^+$  and only 3% and 0.3% by  $\text{K}^+$  and  $\text{Na}^+$ , respectively.

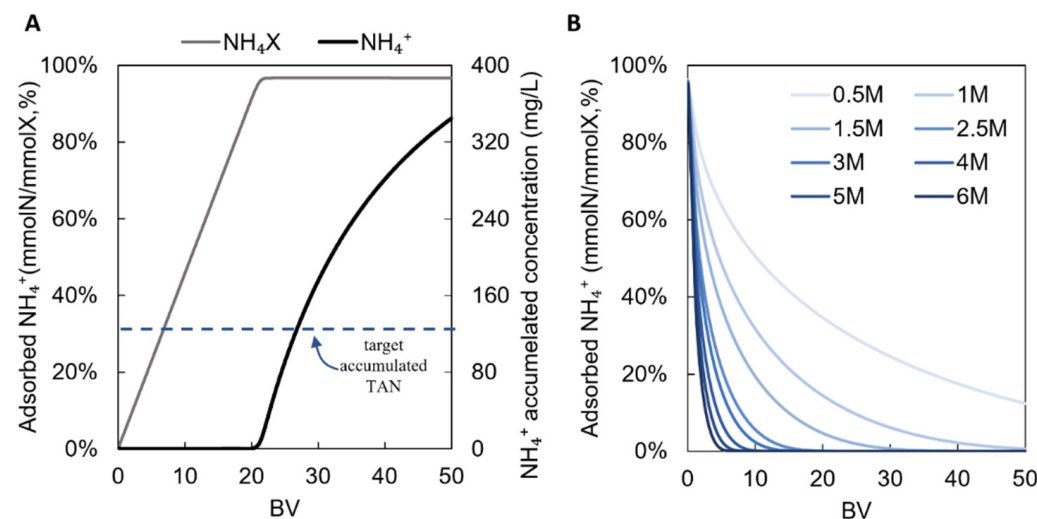


**Figure 5.** (A) Cumulative TAN concentration in the CIX step effluent and the percentage of used adsorption sites of the simulated column; (B) percentage of desorbed TAN of a pre-loaded column using various NaCl concentrations. All simulations were done with the PHREEQC software Transport function, database = phreeqc.dat.

To simulate the regeneration process, different regeneration solution concentrations were tested (Figure 5B). The results show that, by using a 6 M NaCl solution, the resin would be fully regenerated after 6.8 BV, while with a 3 M NaCl solution, the regeneration

would require an 18 BV run. These results were used to determine the initial working conditions in the second part of the work.

### 3.2. Part 2: Selecting the Working Conditions

In the second part, a packed bed column filled with the ZnHCF-composite beads was used (the same beads were used for all the experiments in the second part). The work included several steps aimed at determining the most suitable working conditions (Section 3.2.1) as well as at providing data on the long-term use of the composite beads and the possible reuse of the regeneration solution (Section 3.2.2).

#### 3.2.1. Determining the Most Suitable Hydraulic Retention Time (HRT)

The retention time for the adsorption step was tested to provide data both for the operational capacity and the accumulated TAN concentration in the column's effluent. Figure 6A depicts the results from a preliminary experiment, showing the breakthrough curve of a 40 BV run (0.5 BV/h,  $[TAN]_0 = 640 \text{ mgN/L}$ ). Figure 6A indicates that to reach the target accumulated TAN concentration of 120 mgN/L a ~25 BV cycle is required. This result resembles the simulation prediction presented in Section 3.1.2 (Figure 5A). For the testing of the suitable HRT, a 22 BV adsorption step was conducted (~10% reduction from the preliminary results as a safety factor). In Figure 6B, the breakthrough curves obtained with various HRT are shown, demonstrating that at a flow rate of up to 4 BV/h, the TAN concentration threshold is not reached. The operational capacity (OC) at the end of each tested flow rate was also determined and is listed in Table 4. This value was calculated using the final capacity obtained from the Langmuir isotherm of the ZnHCF performed in DIW (28.52 mgN/gZnHCF and a column packed with 195 g of ZnHCF). A very high OC was observed (>80%) up to a flow rate of 4 BV/h, although a slight, to-be-expected, deterioration in the breakthrough curve was observed in the 4 BV/h experiment and more prominently, in the 8 BV/h breakthrough curve.

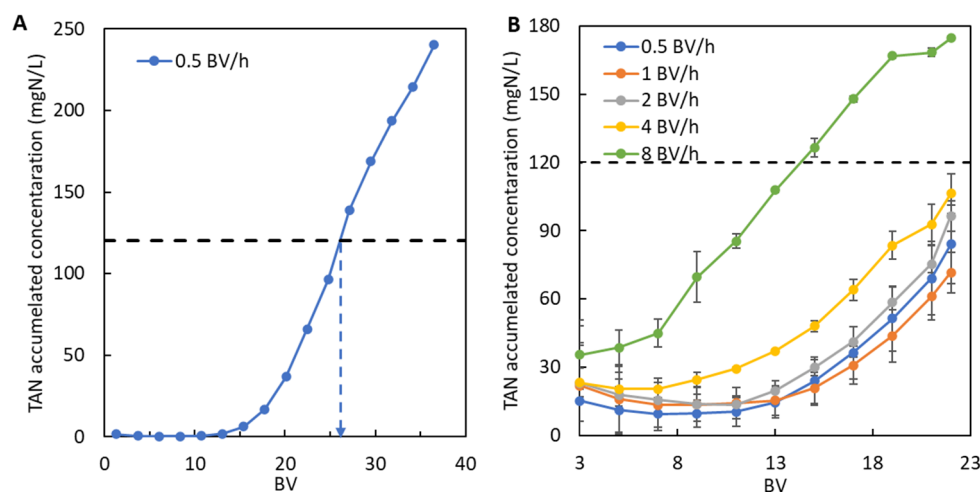


**Figure 6.** (A) shows the breakthrough curve of a preliminary experiment (0.5 BV/h, TAN = 640 mgN/L), and (B) breakthrough curves showing the average cumulative TAN concentration of adsorption effluent as a function of the flow rate for the selected retention times; 22 BV, repetitions ( $n$ ) = 3, and ambient temperature.

**Table 4.** Adsorbed mass and calculated operational capacity at the tested flow rates (22 BV,  $[TAN]_0 = 600 \text{ mgN/L}$ ).

Flow Rate BV/h	Adsorbed Mass of TAN in the Column		Operational Capacity %
	mgN		
$\frac{1}{2}$	4904 $\pm$ 226		88.2%
1	4931 $\pm$ 141		88.7%
2	4594 $\pm$ 172		82.6%
4	4531 $\pm$ 51		81.5%
8	4245 $\pm$ 59		76.3%

### 3.2.2. Breakthrough Curves and Regeneration Data

Using the data given in Section 3.2.1, a full set of cycles was performed as follows: (i) an adsorption step of 22 BV; (ii) a regeneration step of 24 BV (3 M NaCl); and (iii) TAN removal step for reuse of the regeneration solution using electrochemical indirect ammonia oxidation.

Synthetic and real WW solutions were used for cycles 1–10 and 11–20, respectively (see Table 2 for solution composition). Figure 7A presents the average results of the adsorption steps of the synthetic and real WW, showing that the 120 mgN/L threshold was met.

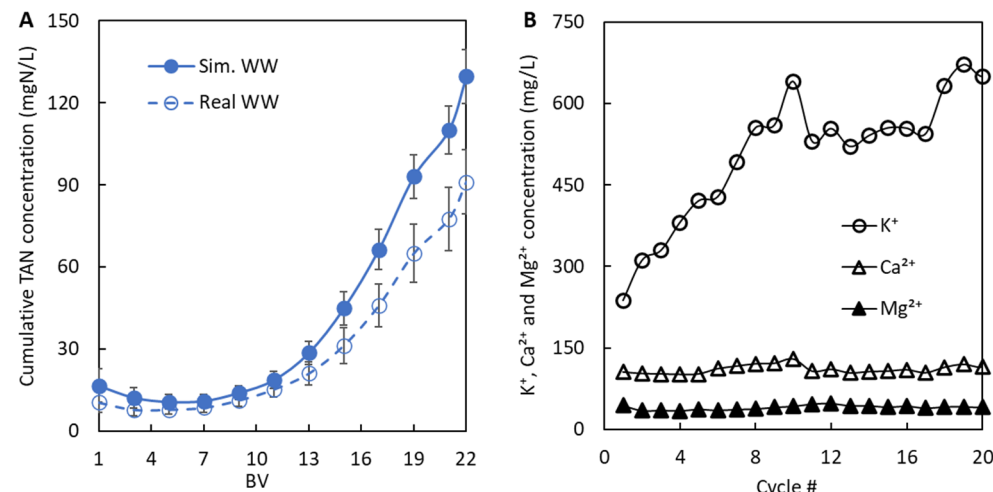


**Figure 7.** (A) Cumulative TAN concentration as a function of the number of bed volumes for the 10 full cycles performed with synthetic wastewater (filled circles), and using the 1st and 2nd batches of real WW (hollow circles). 3 BV/h,  $n = 10$ ; (B) The cations' composition in the exhausted regeneration solution as a function of completed cycles (cycle #1–10 refers to the synthetic experiment, while cycles #11–20 refers to 1st and 2nd batches of real WW experiments).

Figure 7B presents the concentration of the cations ( $\text{Ca}^{2+}$ ,  $\text{Mg}^{2+}$  and  $\text{K}^+$ ) that accumulated in the regeneration solution over time. As can be seen, no change occurred in the concentration of the divalent cations (as their introduction to the regeneration solution was solely through residual water in the column between steps) accompanied by an increase in the  $\text{K}^+$  concentration during the first 10 cycles, which plateaued in cycles 11–17 (batch #1 of real WW), and then another increase (because of the higher  $\text{K}^+$  concentration in RWW #2) followed by another tendency toward a plateau in the last 3 cycles (batch #2 real WW).

In Table 5, the regeneration efficiency is shown for all 20 full cycles, indicating that no deterioration occurred, regardless of the competing ion ( $\text{K}^+$ ) concentration that developed in the regeneration solution, an indication that the main hypothesis of the research, that is, that due to the high affinity of the ZnHCF towards  $\text{NH}_4^+$  ions and zero affinity towards di-valent ions (such as  $\text{Ca}^{2+}$  and  $\text{Mg}^{2+}$ ), the regeneration solution can be reused, practically, for as long as required.

**Table 5.** The results obtained from the breakthrough experiments that were performed using synthetic, and 1st and 2nd batch wastewater as the feed in the adsorption step.

Cycle no.	Synthetic Wastewater				1st and 2nd Batch of Real WW			
	Adsorbed Mass	Desorbed Mass	Regeneration Efficiency	Feed Conc.	Adsorbed Mass	Desorbed Mass	Regeneration Efficiency	Feed Conc.
1	mgN 4383	mgN 4279	% 98%	mgN/L 605	mgN 4513	mgN 3983	% 88%	mgN/L 581
2	4387	4381	100%	606	4568	4055	89%	581
3	4605	4586	100%	602	4037	3817	95%	517
4	4591	4361	95%	603	3956	3719	94%	518
5	4518	4280	95%	610	4047	3741	92%	535
6	4525	4302	95%	621	3940	3762	95%	534
7	4427	4347	98%	604	3905	3937	101%	529
8	4446	4457	100%	603	4060	4096	101%	538
9	4457	4731	106%	603	4208	4078	97%	568
10	4503	4402	98%	603	4038	3955	98%	554
Average	4484	4413	98%	606	4127	3914	95%	545
STDV	74	138		5	222	137		23

#### 4. Cost Assessment

The proposed process (Figure 2) cost was evaluated. Since the first and second steps (TAN adsorption and desorption) are identical, regardless of the treatment that is applied to the regeneration solution, the focus was on the regeneration-solution TAN-removal process. Two methods were examined for the TAN removal: (i) indirect electrochemical ammonia oxidation (which was also performed experimentally in the lab), and (ii) high-pH NH<sub>3</sub> air-stripping for reuse purposes (simulated using the CHEMCAD® software [44]).

Both capital expenditure (CAPEX) and operational expenditure (OPEX) were considered, and the currency used is the US Dollar (USD). For the CAPEX evaluation, the construction of a CIX column that includes all the various parts (material, civil engineering, design, etc.) was adopted from [45] as 14,054 \$/m<sup>3</sup> of column volume. The price of the ZnHCF composite material was estimated at 50 \$/kg, taking a safety factor from the price estimated in [33] as the global prices of all commodities have risen recently; an annual replacement of 5% of the ZnHCF was assumed, and a three-column setup was chosen for the semi-continuous operation of the CIX step. The costs were normalized to 1 m<sup>3</sup> of treated wastewater entering the WWTP (\$¢/m<sup>3</sup>, USD), by assuming a lifespan of 20 years and a 5% interest.

For the OPEX calculation, two TAN-removal methods were assessed. For method (i), the energy demand for the electrolyzer was calculated with 90% current efficiency and 3.3 V of applied potential (as applied in the current work); the energy demand of the pumps, and for mixing and aeration was assumed to be 80% of the energy requirement of the electrolyzer.

For method (ii), the energy demands for heating the solution, the stripping air, and operating the pumps and the heat exchangers were obtained from the CHEMCAD® simulation. The cost of grid electricity was estimated at 0.0807 \$/kWh [46]. The cost of NaOH (\$700/ton) was added at a 1:1 molar ratio with the TAN concentration [13] and 0.5% per cycle NaCl (\$220/ton, [47]) was assumed to compensate for losses between cycles. For the stripping step (method (ii)), an addition of 1:1.05 molar of NaOH was assumed (to reach pH~10.5), the price of HCl was assumed at 98 \$/ton (NH<sub>3(g)</sub> receiving solution), and the product solution price of the obtained NH<sub>4</sub>Cl was estimated at 1200 \$/ton [47].

For the cost estimation, the case study of the Shafdan (Israel) WWTP [48] was adopted, with a daily inlet flow rate of 380,000 m<sup>3</sup>/d, and a ~1% flow rate of the supernatant stream, assuming a reduction of 500 mgN/L in this stream by the investigated process.

The cost analysis results are presented in Table 6, in which both TA-removal methods are compared, showing almost similar results for the electrolysis and stripping methods of 3.29 and 3.26 USD cents per m<sup>3</sup> of treated wastewater that enters the WWTP, respectively. Reusing the ammonia gas by using a scrubber and producing an NH<sub>4</sub>Cl solution, may add a retail value (normalized to m<sup>3</sup> of treated wastewater) of ~1 USD cents per m<sup>3</sup>, to render

the final overall cost of the stripping treatment to be 2.26 USD cents per  $\text{m}^3$ , making this alternative the more economical choice.

**Table 6.** Cost analysis of the proposed process, showing the analysis for the two proposed methods for TAN removal from the exhausted regeneration solution.

	Parameter	Unit	Method #1—Electrolysis	Method #2—Stripping
OPEX	NaOH	\$¢/m <sup>3</sup>	1.00	1.05
	NaCl	\$¢/m <sup>3</sup>	0.19	0.19
	ZnHCF	\$¢/m <sup>3</sup>	0.24	0.24
	Energy	\$¢/m <sup>3</sup>	1.53	1.45
CAPEX	Columns	\$¢/m <sup>3</sup>	0.13	0.13
	ZnHCF	\$¢/m <sup>3</sup>	0.19	0.19
	OPEX	\$¢/m <sup>3</sup>	2.96	2.94
	CAPEX	\$¢/m <sup>3</sup>	0.32	0.32
<b>Total cost</b>		<b>\$¢/m<sup>3</sup></b>	<b>3.29</b>	<b>3.26</b>

At this price range, which is much higher than the cost of biological nitrogen removal, it would make sense to apply the proposed method where either no biological treatment is possible (due to the presence of toxic constituents, noncontinuous flow, or low temperature; one possible example being landfill leachates), or, more relevant to the case of a municipal WWTP, to allow increasing the organic matter load on the oxidizing reactor by up to 10–15%, without increasing the ammonia load on it.

## 5. Conclusions

A new cation-exchange-based ammonia separation (and reuse) technology from the supernatant line in municipal wastewater treatment plants is presented. To be economically feasible, the regeneration solution must be reused for many cycles, which means that the ion exchange material should have a very high affinity toward  $\text{NH}_4^+$  along with a very low affinity toward competing ions, particularly divalent cations. The use of PES-coated ZnHCF beads was exemplified for this purpose in the work. The hypothesis was that the very high affinity of this adsorbent toward  $\text{NH}_4^+$  will allow the reuse of the regeneration solution for many cycles without the intervention of competing cations, which will not be adsorbed by the ZnHCF and thus not released into the regeneration solution. The results show that, indeed, the regeneration solution was hardly contaminated with competing cations, and that the breakthrough curves did not deteriorate at all after 20 adsorption/regeneration cycles while operating with a flow rate of 3 BV/h. The cost of separating and reusing the ammonia as an  $\text{NH}_4\text{Cl}$  solution was approximated at \$0.02/m<sup>3</sup> of influent wastewater, making it cost-effective mostly in cases when the WWTP receives a higher-than-planned load and an incentive exists for alleviating the TAN load on the oxidation reactor. Nevertheless, the described process can be cost-effective for removing/reusing ammonia from streams that cannot be treated biologically, such as landfill leachates or certain (toxic) industrial wastes. Further work should concentrate on applying the described technique to such solutions and/or for adsorbing  $\text{NH}_4^+$  from the effluents of WWTPs, as a polishing method, when the main ammonia oxidation process is not entirely efficient.

**Author Contributions:** P.N.: Methodology, Data curation, Writing original draft, Visualization, Validation, Writing review and editing. Z.A.D.: Methodology, Data curation, Writing original draft, Validation, Writing review and editing. C.D.-J.: Methodology, Data curation, Software, Visualization, Validation, Writing review and editing. Y.A.: Data curation, Visualization, Software, Validation, Writing review and editing. R.B.-A.: Data curation, Visualization, Validation, Writing review and editing. O.L.: Conceptualization, Writing original draft, Supervision, Writing review and editing, Visualization, Funding acquisition. All authors have read and agreed to the published version of the manuscript.

**Funding:** This research was partially funded by MOST-BMBF: The German–Israeli Water Technology Cooperation Program, grant number 3-17764.

**Data Availability Statement:** Not applicable.

**Conflicts of Interest:** The authors declare no conflict of interest.

## Appendix A

The Langmuir isotherm equation is given by Equation (A1):

$$q_e = \frac{Q_{e\max}}{1 + K_L \cdot [C_e]} \quad (\text{A1})$$

where  $q_e$  is the amount of adsorbate adsorbed at the equilibrium (mg/g);  $C_e$  is the supernatant adsorbate concentration at the equilibrium (mg/L);  $K_L$  is the Langmuir equilibrium constant (L/mg); and  $Q_{\max}$  is the maximum adsorption capacity of the adsorbent (mg/g).

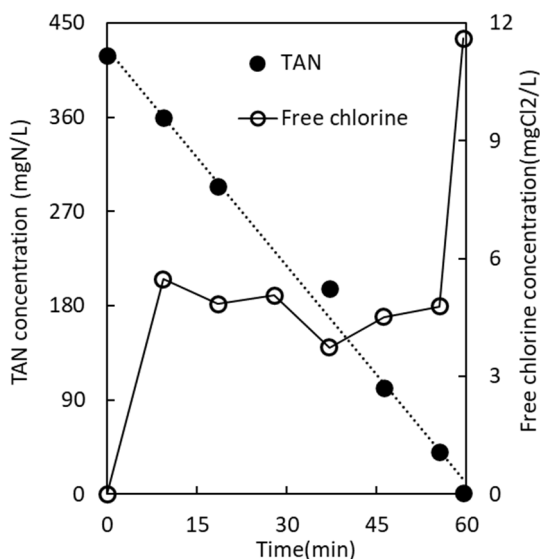


**Figure A1.** Free chlorine and total ammonia nitrogen (TAN) concentration over time during an electrolysis run on the 2nd batch of real wastewater (WW) experiment, cycle #3, with a current efficiency of 92.9% ( $I = 26.1 \text{ A}$ ,  $V = 3.3 \text{ V}$ ).

## References

- Ronan, E.; Aqeel, H.; Wolfaardt, G.M.; Liss, S.N. Recent Advancements in the Biological Treatment of High Strength Ammonia Wastewater. *World J. Microbiol. Biotechnol.* **2021**, *37*, 158. [[CrossRef](#)] [[PubMed](#)]
- Sheng, L.; Lei, Z.; Dzakpasu, M.; Li, Y.-Y.; Li, Q.; Chen, R. Application of the Anammox-Based Process for Nitrogen Removal from Anaerobic Digestion Effluent: A Review of Treatment Performance, Biochemical Reactions, and Impact Factors. *J. Water Process Eng.* **2020**, *38*, 101595. [[CrossRef](#)]
- Zhao, Q.; Peng, Y.; Li, J.; Gao, R.; Jia, T.; Deng, L.; Du, R. Sustainable Upgrading of Biological Municipal Wastewater Treatment Based on Anammox: From Microbial Understanding to Engineering Application. *Sci. Total Environ.* **2022**, *813*, 152468. [[CrossRef](#)]
- Zhao, J.; Zuo, J.; Lin, J.; Li, P. The Performance of a Combined Nitritation-Anammox Reactor Treating Anaerobic Digestion Supernatant under Various C/N Ratios. *J. Environ. Sci.* **2015**, *30*, 207–214. [[CrossRef](#)]
- Cao, S.; Yan, W.; Yu, L.; Zhang, L.; Lay, W.; Zhou, Y. Challenges of THP-AD Centrate Treatment Using Partial Nitritation-Anammox (PN/A)—Inhibition, Biomass Washout, Low Alkalinity, Recalcitrant and More. *Water Res.* **2021**, *203*, 117555. [[CrossRef](#)]
- Shih, K.; Yan, H. Chapter 26—The Crystallization of Struvite and Its Analog K-Struvite; From Waste Streams for Nutrient Recycling; Elsevier Inc.: Amsterdam, The Netherlands, 2016; ISBN 9780128038376.
- Wu, H.; Vaneeckhaute, C. Nutrient Recovery from Wastewater: A Review on the Integrated Physicochemical Technologies of Ammonia Stripping, Adsorption and Struvite Precipitation. *Chem. Eng. J.* **2022**, *433*, 133664. [[CrossRef](#)]
- Lahav, O.; Telzhensky, M.; Zewuhn, A.; Gendel, Y.; Gerth, J.; Calmano, W.; Birnhack, L. Struvite Recovery from Municipal-Wastewater Sludge Centrifuge Supernatant Using Seawater NF Concentrate as a Cheap Mg(II) Source. *Sep. Purif. Technol.* **2013**, *108*, 103–110. [[CrossRef](#)]
- Huang, K.-L. Removal of Organic and Ammonium Nitrogen Pollutants in Swine Wastewater Using Electrochemical Advanced Oxidation. *Int. J. Electrochem. Sci.* **2018**, *13*, 11418–11431. [[CrossRef](#)]
- Deng, Y.; Zhao, R. Advanced Oxidation Processes (AOPs) in Wastewater Treatment. *Curr. Pollut. Rep.* **2015**, *1*, 167–176. [[CrossRef](#)]

11. Tanaka, H.; Fujimoto, M.; Minami, K.; Takahashi, A.; Parajuli, D.; Hiwatari, T.; Kawakami, M.; Kawamoto, T. Ammonium Removal and Recovery from Sewage Water Using Column-System Packed Highly Selective Ammonium Adsorbent. *Environ. Pollut.* **2021**, *284*, 117495. [[CrossRef](#)]
12. Thornton, A.; Pearce, P.; Parsons, S.A. Ammonium Removal from Digested Sludge Liquors Using Ion Exchange. *Water Res.* **2007**, *41*, 433–439. [[CrossRef](#)] [[PubMed](#)]
13. Lahav, O.; Schwartz, Y.; Nativ, P.; Gendel, Y. Sustainable Removal of Ammonia from Anaerobic-Lagoon Swine Waste Effluents Using an Electrochemically-Regenerated Ion Exchange Process. *Chem. Eng. J.* **2013**, *218*, 214–222. [[CrossRef](#)]
14. Cydzik-Kwiatkowska, A.; Zielińska, M. Bacterial Communities in Full-Scale Wastewater Treatment Systems. *World J. Microbiol. Biotechnol.* **2016**, *32*, 66. [[CrossRef](#)] [[PubMed](#)]
15. Miłobędzka, A.; Witeska, A.; Muszyński, A. Factors Affecting Population of Filamentous Bacteria in Wastewater Treatment Plants with Nutrients Removal. *Water Sci. Technol.* **2016**, *73*, 790–797. [[CrossRef](#)]
16. Speirs, L.B.M.; Rice, D.T.F.; Petrovski, S.; Seviour, R.J. The Phylogeny, Biodiversity, and Ecology of the Chloroflexi in Activated Sludge. *Front. Microbiol.* **2019**, *10*, 02015. [[CrossRef](#)]
17. Guida, S.; van Peteghem, L.; Luqmani, B.; Sakarika, M.; McLeod, A.; McAdam, E.J.; Jefferson, B.; Rabaey, K.; Soares, A. Ammonia Recovery from Brines Originating from a Municipal Wastewater Ion Exchange Process and Valorization of Recovered Nitrogen into Microbial Protein. *Chem. Eng. J.* **2022**, *427*, 130896. [[CrossRef](#)]
18. Tanaka, J.; Matsumura, M. Application of Ozone Treatment for Ammonia Removal in Spent Brine. *Adv. Environ. Res.* **2003**, *7*, 835–845. [[CrossRef](#)]
19. Gendel, Y.; Lahav, O. Revealing the Mechanism of Indirect Ammonia Electrooxidation. *Electrochim. Acta* **2012**, *63*, 209–219. [[CrossRef](#)]
20. Ben-Asher, R.; Stefánsson, G.; Ólafsdóttir, A.; Mayer, H.; Nahir, R.; Gendel, Y.; Lahav, O. On-Board Zero-Discharge Water Treatment Unit for Well-Boats: Arctic Char as a Case Study. *J. Appl. Aquac.* **2022**, *34*, 953–968. [[CrossRef](#)]
21. Lubensky, J.; Ellersdorfer, M. Pilot Scale Experiments for Ammonium Recovery from Sludge Liquor at a Municipal Waste Water Treatment Plant. *J. Sustain. Dev. Energy Water Environ. Syst.* **2021**, *9*, 1080349. [[CrossRef](#)]
22. Lubensky, J.; Ellersdorfer, M.; Stocker, K. Ammonium Recovery from Model Solutions and Sludge Liquor with a Combined Ion Exchange and Air Stripping Process. *J. Water Process Eng.* **2019**, *32*, 100909. [[CrossRef](#)]
23. Pesonen, J.; Myllymäki, P.; Tuomikoski, S.; Vervecken, G.; Hu, T.; Prokkola, H.; Tynjälä, P.; Lassi, U. Use of Calcined Dolomite as Chemical Precipitant in the Simultaneous Removal of Ammonium and Phosphate from Synthetic Wastewater and from Agricultural Sludge. *ChemEngineering* **2019**, *3*, 40. [[CrossRef](#)]
24. Lahav, O.; Green, M. Ammonium Removal Using Ion Exchange and Biological Regeneration. *Water Res.* **1998**, *32*, 2019–2028. [[CrossRef](#)]
25. Pabalan, R.T.; Bertetti, F.P. Cation-Exchange Properties of Natural Zeolites. *Rev. Miner. Geochem.* **2001**, *45*, 453–518. [[CrossRef](#)]
26. Barrer, R.M.; Davies, J.A.; Rees, L.V.C. Thermodynamics and Thermochemistry of Cation Exchange in Chabazite. *J. Inorg. Nucl. Chem.* **1969**, *31*, 219–232. [[CrossRef](#)]
27. Piernas Muñoz, M.J.; Castillo Martínez, E. *Prussian Blue Based Batteries*; Springer International Publishing: Cham, Switzerland, 2018; ISBN 978-3-319-91487-9.
28. Zhang, L.; Chen, L.; Zhou, X.; Liu, Z. Morphology-Dependent Electrochemical Performance of Zinc Hexacyanoferrate Cathode for Zinc-Ion Battery. *Sci. Rep.* **2015**, *5*, 18263. [[CrossRef](#)]
29. Wang, J.; Zhuang, S.; Liu, Y. Metal Hexacyanoferrates-Based Adsorbents for Cesium Removal. *Coord. Chem. Rev.* **2018**, *374*, 430–438. [[CrossRef](#)]
30. Naidu, G.; Nur, T.; Loganathan, P.; Kandasamy, J.; Vigneswaran, S. Selective Sorption of Rubidium by Potassium Cobalt Hexacyanoferrate. *Sep. Purif. Technol.* **2016**, *163*, 238–246. [[CrossRef](#)]
31. Jiang, Y.; Minami, K.; Sakurai, K.; Takahashi, A.; Parajuli, D.; Lei, Z.; Zhang, Z.; Kawamoto, T. High-Capacity and Selective Ammonium Removal from Water Using Sodium Cobalt Hexacyanoferrate. *RSC Adv.* **2018**, *8*, 34573–34581. [[CrossRef](#)]
32. Shakir, K.; Sohsah, M.; Soliman, M. Removal of Cesium from Aqueous Solutions and Radioactive Waste Simulants by Coprecipitate Flotation. *Sep. Purif. Technol.* **2007**, *54*, 373–381. [[CrossRef](#)]
33. Nativ, P.; Ben-Asher, R.; Fridman-Bishop, N.; Lahav, O. Synthesis and Characterization of Zinc-Hexacyanoferrate Composite Beads for Controlling the Ammonia Concentration in Low-Temperature Live Seafood Transports. *Water Res.* **2021**, *203*, 117551. [[CrossRef](#)] [[PubMed](#)]
34. Metcalf & Eddy Inc. *Wastewater Engineering: Treatment and Resource Recovery*, 5th ed.; McGraw-Hill Professional: New York, NY, USA, 2013.
35. Britton, A.; Koch, F.A.; Mavinic, D.S.; Adnan, A.; Oldham, W.K.; Udal, B. Pilot-Scale Struvite Recovery from Anaerobic Digester Supernatant at an Enhanced Biological Phosphorus Removal Wastewater Treatment Plant. *J. Environ. Eng. Sci.* **2005**, *4*, 265–277. [[CrossRef](#)]
36. Takahashi, A.; Kitajima, A.; Parajuli, D.; Hakuta, Y.; Tanaka, H.; Ohkoshi, S.; Kawamoto, T. Radioactive Cesium Removal from Ash-Washing Solution with High PH and High K+-Concentration Using Potassium Zinc Hexacyanoferrate. *Chem. Eng. Res. Des.* **2016**, *109*, 513–518. [[CrossRef](#)]

37. Bergmann, C.P.; Machado, F.M. Part of the book series: *Carbon Nanostructures (CARBON)*. *Carbon Nanomaterials as Adsorbents for Environmental and Biological Applications*; Bergmann, C.P., Machado, F.M., Eds.; Carbon Nanostructures; Springer International Publishing: Cham, Switzerland, 2015; ISBN 978-3-319-18874-4.
38. Langmuir, I. The Adsorption of Gases on Plane Surfaces of Glass, Mica and Platinum. *J. Am. Chem. Soc.* **1919**, *40*, 1361–1403. [CrossRef]
39. Marei, S.A.; Basahel, S.N.; Rahmatallah, A.B. Ammonium Ion Exchange Equilibrium on Potassium Zinc Hexacyanoferrate/II/ $K_2Zn_3[Fe/CN/6]_2$ . *J. Radioanal. Nucl. Chem. Lett.* **1986**, *104*, 217–222. [CrossRef]
40. Charlton, S.R.; Parkhurst, D.L. Modules Based on the Geochemical Model PHREEQC for Use in Scripting and Programming Languages. *Comput. Geosci.* **2011**, *37*, 1653–1663. [CrossRef]
41. Willis, R.B.; Montgomery, M.E.; Allen, P.R. Improved Method for Manual, Colorimetric Determination of Total Kjeldahl Nitrogen Using Salicylate. *J. Agric. Food Chem.* **1996**, *44*, 1804–1807. [CrossRef]
42. Vlasselaer, S.; D'Olieslager, W.; D'Hont, M. Caesium Ion Exchange Equilibrium on Potassium-Zinc-Hexacyanoferrate(II)  $K_2Zn_3(Fe(CN)_6)_2$ . *J. Inorg. Nucl. Chem.* **1976**, *38*, 327–330. [CrossRef]
43. Crittenden, J.C.; Trussell, R.R.; Hand, D.W.; Howe, K.J.; Tchobanoglous, G. *MWH's Water Treatment*; John Wiley & Sons, Inc.: Hoboken, NJ, USA, 2012; ISBN 9781118131473.
44. CHEMCAD, V8.1.0.16649 by Chemstations, Inc. Available online: <https://www.chemstations.com> (accessed on 24 November 2022).
45. Gräber, Y.; Nativ, P.; Lahav, O. A Pre-Treatment Concept for Increasing the Recovery Ratio of Coastline BWRO Plants, While Providing  $Mg^{2+}$  in the Product Water. *Desalination* **2021**, *515*, 115202. [CrossRef]
46. Electric Power Monthly—U.S. Energy Information Administration (EIA). Available online: [https://www.eia.gov/electricity/monthly/epm\\_table\\_grapher.php?t=table\\_5\\_03](https://www.eia.gov/electricity/monthly/epm_table_grapher.php?t=table_5_03) (accessed on 4 April 2021).
47. Price of Industrial Salt in the United States from 2016 to 2021, by Type. Available online: <https://www.Statista.Com/Statistics/916733/Us-Salt-Prices-by-Type/> (accessed on 24 November 2022).
48. Nativ, P.; Gräber, Y.; Aviezer, Y.; Lahav, O. A Simple and Accurate Approach for Determining the VFA Concentration in Anaerobic Digestion Liquors, Relying on Two Titration Points and an External Inorganic Carbon Analysis. *ChemEngineering* **2021**, *5*, 15. [CrossRef]